Available online at www.eccomasproceedia.org
Eccomas Proceedia COMPDYN (2017) 1590-1605

ECCOMAS
Proceedia

COMPDYN 2017
6th ECCOMAS Thematic Conference on
Computational Methods in Structural Dynamics and Earthquake Engineering
M. Papadrakakis, M. Fragiadakis (eds.)
Rhodes Island, Greece, 15–17 June 2017

CYCLIC RESPONSE AND NONLINAR MODELING OF EXTERIOR UNREINFORCED RC BEAM-COLUMN JOINTS WITH PLAIN LONGITUDINAL BARS

Maria Teresa De Risi[1], **Paolo Ricci**[1], **Gerardo Mario Verderame**[1]

[1] University of Naples Federico II, Department of Structures for Engineering and Architecture
via Claudio, 21 - 80125 Naples
mariateresa.derisi@unina.it, paolo.ricci@unina.it, verderam@unina.it

Keywords: existing RC buildings, unreinforced beam-column joints, plain bars, experimental tests, nonlinear modelling, bond-slip.

Abstract. *The seismic performance of existing Reinforced Concrete (RC) frames is significantly affected by the behaviour of beam-column intersections involved in the collapse mechanism, especially in non-conforming buildings with poor structural detailing or completely unreinforced joints. Even if a quite significant amount of studies on seismic performance of unreinforced joints has been carried out in last years, a very limited number of them deals with specimens reinforced with plain hook-ended longitudinal bars, widespread in Italian and Mediterranean building stock, or with the analysis of local aspects, such as the evaluation of joint shear strains. The majority of the models proposed in literature to simulate the cyclic behaviour of RC joints were developed and calibrated by means of tests performed on elements with deformed bars. Thus, these models may be not adequate for elements with hook-ended plain bars, especially due to the peculiarities in the interaction mechanisms between concrete and steel for this bar typology.*

This study first analyses the cyclic experimental tests of four full-scale exterior unreinforced RC beam-column joints with longitudinal plain bars in beams and columns carried out by the authors, in continuity with a previous experimental campaign. The specimens mainly differ for joint aspect ratio and beam longitudinal reinforcement ratio. Global and local responses of such tests are analyzed. The joint deformation mechanisms – rotation at the interface between beam/columns and joint, and shear deformation of the joint panel – are also analyzed. Then, a numerical modelling approach is carried out by OpenSees software to reproduce the experimental cyclic response. Bond-slip is particularly taken into account by introducing a slip spring whose properties are calculated using a bond-slip model properly proposed in literature for plain bars. The numerical results are presented and finally compared with the experimental results highlighting the influence of nonlinear response of joint panel and bond-slip mechanism in the response of the sub-assemblage.

Peer-review under responsibility of the organizing committee of COMPDYN 2017.
doi: 10.7712/120117.5515.17511

1 INTRODUCTION

Reinforced Concrete (RC) buildings designed according to obsolete seismic codes or for gravity loads only are widespread in Italian and Mediterranean building stock. For these buildings, beam-column joints can represent a critical issue, leading to shear failures that limit the achievement of the flexural capacity of the adjoining members ([1]-[2]). As a matter of fact, past earthquakes showed that shear failures in beam-column joints can lead to building collapse ([3]-[5]) mainly due to the inadequate joint confinement, in particular for structures designed for gravity loads only.

A significant amount of studies has been carried out in last years on seismic performance of unreinforced beam-column joints (e.g. [6]-[10]). These researches have focused the attention on the effect of different parameters on seismic performance of joints without stirrups in the joint core – in particular including the effect of column axial load, concrete strength, joint aspect ratio, or beam longitudinal reinforcement ratio – but very few of them handled with specimens with plain hook-ended longitudinal bars, widespread in the existing RC building stock of the Mediterranean region. As a result, despite a certain amount of recent experimental tests on exterior joints, the number of tests performed on RC unreinforced joints built with plain bars is certainly very low (see [12]) if compared with the available data for RC joints with deformed bars [13]. Moreover, there is a great inhomogeneity (e.g. for anchorage details, or presence of slab or ties in the joint core) in test campaigns carried out all around the word and representing different constructive practices, typical of each country. Researchers often focused their attention mainly on the shear strength of the joint panel; thus, only few of them provided experimental values of joint shear strains, nevertheless the crucial role of this data to reproduce joint performance in numerical modelling in a reliable way. Furthermore, only two shear strength models ([14]-[15]) exist in literature for this joint typology.

This study first analyses the cyclic experimental tests on four full-scale exterior unreinforced RC beam-column joints with longitudinal plain bars in beams and columns carried out by the authors, in continuity with a previous experimental campaign [12]. The specimens are mainly different for joint aspect ratio and beam longitudinal reinforcement ratio. Global and local responses of such tests are analyzed. The different joint deformation mechanisms – rotation at the interface between beam/columns and joint, and shear deformation of the joint panel – are also investigated. Then, a numerical modelling is carried out by OpenSees software platform to reproduce the experimental cyclic response. Bond-slip is particularly taken into account by introducing a slip spring whose properties are calculated using a bond-slip model properly proposed in literature for plain bars. The numerical results are presented and finally compared with the experimental results highlighting the influence of nonlinear response of joint panel and bond-slip mechanism in the response of the sub-assemblage.

2 EXPERIMENTAL CAMPAIGN

Four full-scale exterior unreinforced beam-column sub-assemblages have been designed and tested under cyclic loading. All the specimens are reinforced with hook-ended plain longitudinal rebars. Columns (top and bottom) have a square cross-section with height (h_c) and width (b_c) equal to 30 cm for all the specimens (see Figure 1). The four tests are different for joint aspect ratio (h_b/h_c) and beam longitudinal reinforcement amount (A_{sb}), in order to observe and analyze the effect of such parameters on joint shear strength and deformability. In particular, beam sectional area is rectangular with 30 cm depth (b_b=30 cm) for all the specimens; whereas the beam height (h_b) is equal to 40 cm for Tests #1bP and #2bP, and 60 cm for Test #1cP and #2cP (Figure 1). Thus, joint aspect ratio results to be equal to 1.33 or 2.00, respectively, depending on beam height. Column length was designed to be representative of

typical interstorey height (3.40m), so that column shear length, L_c (up to the centerline of the beam), is equal to 1.70 m. The beam length, L_b (up to the centerline of the column) is equal to 1.80 m (Figure 1).

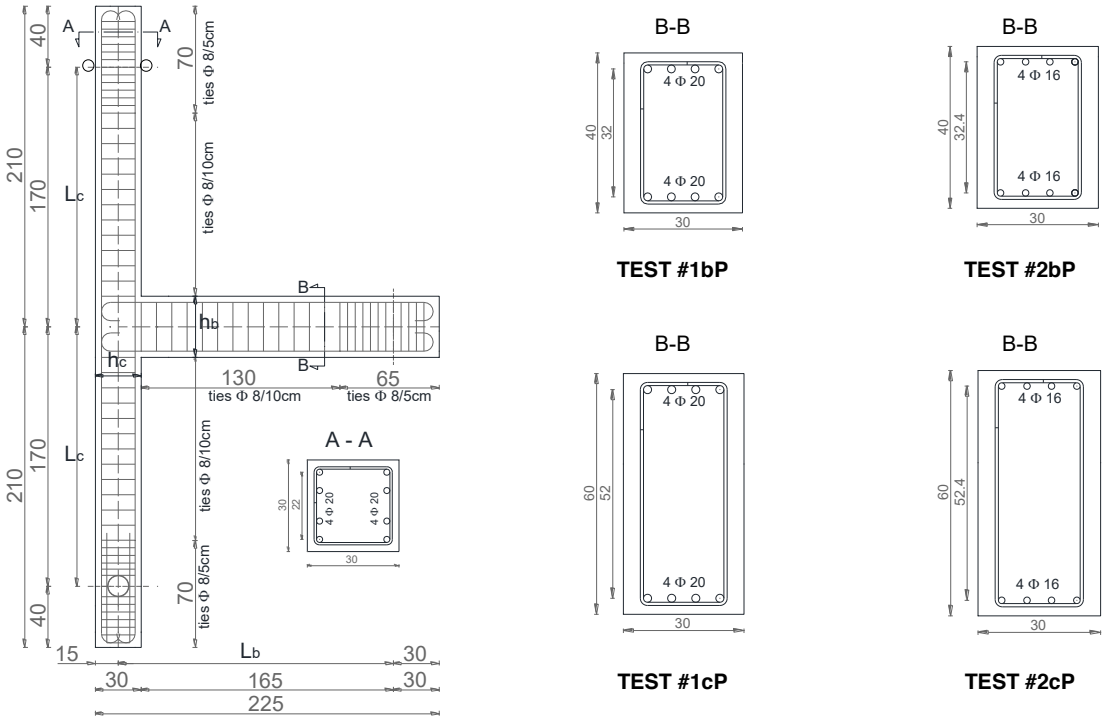

Figure 1: Geometry (dimensions in cm) and reinforcement details.

Beam longitudinal reinforcement is higher for Tests #1bP and #1cP (symmetrically reinforced with 4ϕ20) with respect to Tests #2bP and #2cP (symmetrically reinforced with 4ϕ16). Column longitudinal reinforcement consists of 4ϕ20 for both the reinforcement layers so that a weak beam-strong column hierarchy is obtained. The longitudinal reinforcement in the columns extends continuously up through the joint from the bottom to the top of the column. Transverse reinforcement in beams and columns was designed to avoid shear failures, to not preclude joint shear failure, which is the focus of this work. No transverse reinforcement was located in the joint panel zone, in compliance with code prescriptions in force in the Mediterranean area until ’80, also in regions with high seismic hazard. Top and bottom beam longitudinal bars are anchored with end hooks bent inside the joint core: the internal curvature radius of the hooks is equal to 2.5 times the bar diameter (according to the Italian constructive practice in force until 70’s). The transverse reinforcement in beams and columns consists of 8 mm diameter closed stirrups with 90° bent and 10 cm extension on both ends. The stirrups are spaced at 10 cm along the beam and the column except within beam and column ends, where the spacing is reduced to 5 cm to give adequate strength at the location where forces are applied during the test.

Concrete compressive strength (f_c) was evaluated on four 15×15×15cm^3 cubic samples (CSs) of the casted concrete. Values of 28-day cylindrical strength for each CS have been calculated as 0.83 times the cubic strength (according to [16]), and their mean value is equal to 17.7 MPa. Mechanical properties of the reinforcing steel for plain longitudinal reinforcement are similar to AQ42 or FeB22k commercial typologies (very commonly employed in Italy between ‘60s and ‘70s). Tensile tests were carried out on three samples for each bar diameter. Mean values of their yield strength, f_y, are equal to 370 MPa for 20 mm bar diameter and 330

MPa for 16 mm bar diameter. Mean values of their ultimate strength, f_t, are equal to 520 MPa and 446 MPa, for 20 mm and 16 mm bar diameter, respectively. Deformed bars B450C (i.e., class C reinforcement with f_{yk}=450 MPa according to Annex C provisions of Eurocode 2) were adopted for transverse reinforcement in beams and columns, for sake of convenience.

A schematic of the loading apparatus is shown in Figure 2. The column was mounted with pinned supports at both ends. A constant value of axial load equal to N=160 kN (corresponding to an axial load ratio equal to ν=0.10) was applied. A hydraulic actuator applied the lateral load in displacement control at the end of the beam by means of a loading collar. A wire potentiometer was placed at the end of the beam to monitor beam deflection. Ten Linear Potentiometer sensors (LPs) adopted to measure joint shear strains and cracks width at column-joint interfaces were located in the joint panel along longitudinal reinforcement layers of beam and columns and along the diagonals of the joint panel, as shown in Figure 2. Two additional Linear Variable Displacement Transducers (LVDTs) located along the beam depth were used in order to measure cracks width at beam-joint interface. Strains in beam longitudinal reinforcement were measured, too, by means of two strain gauges (sg) located at beam-joint interface, as shown in Figure 2.

Before beginning each test, the axial load was slowly applied to the column until the appropriate level was achieved. Then, the lateral load was cyclically applied, in a quasi-static way, at the end of the beam. The loading procedure consisted of displacement-controlled steps beginning at a 0.25% drift followed by steps of 0.50%, 0.75%, 1.00%, 1.50%, 2.00%, 3.00%, 4.00% and 6.00% drift. Each drift step consisted of three push-pull cycles. Hereinafter, the term drift will represent the ratio between the imposed displacement (Δ_b) and beam length (from the loaded end to the column centerline), namely, drift = Δ_b/L_b.

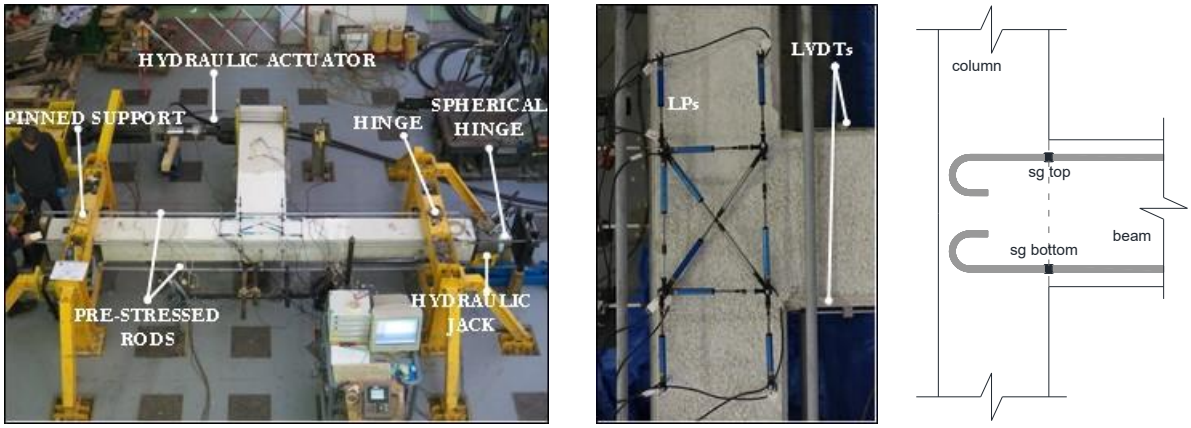

Figure 2: Test setup, joint panel instrumentation, and strain gauges location.

3 EXPERIMENTAL RESULTS

3.1 Beam load-displacement responses

The response in terms of beam lateral load (V_b) versus drift is reported in Figure 3 for all the tests together with the convention adopted for signs of load and displacement. Generally speaking, the experimental response during the push-pull cycles appears quite symmetric for all the tests, except for the case of Test #1cP that shows a bit higher difference in terms of maximum achieved beam load between positive and negative loading directions.

In particular, for all the specimens, the maximum beam load achieved during the test (equal to 51.7 kN, 50.3 kN, 68.4 kN, 46.9 kN, respectively for Tests #1bP, #2bP, #1cP, #2cP) is lower than the expected beam load at yielding (equal to 89.6 kN, 52.5 kN, 143.5 kN, 83.6

kN, respectively for Tests #1bP, #2bP, #1cP, #2cP). Therefore, the joint panel failure is nominally defined as J-failure mode (i.e. joint shear failure without yielding of the adjacent members). This observed failure typology is also confirmed by the measures of strains of the longitudinal bars of the beam (located as shown in Figure 2), which provided maximum values of steel strain that are always lower than the expected strain corresponding to yielding for each bar.

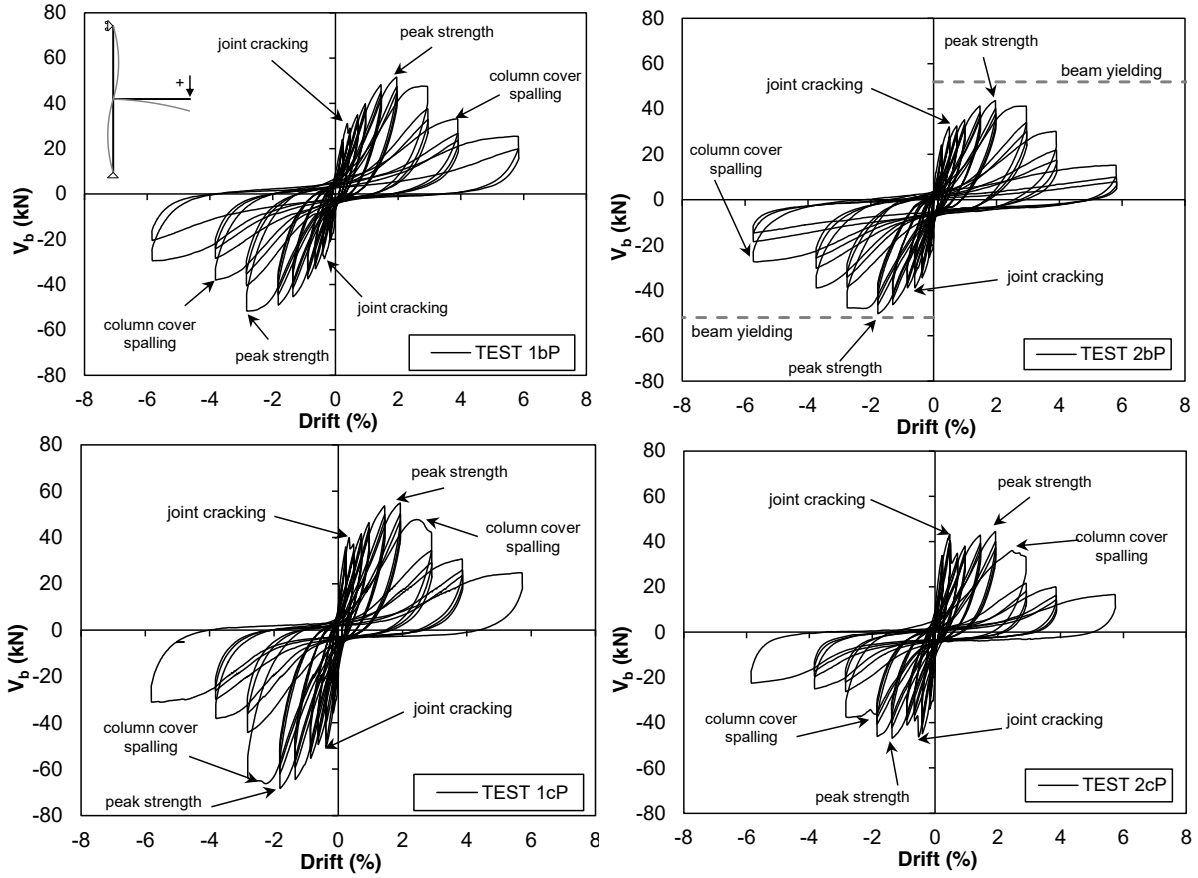

Figure 3: Global experimental responses: beam lateral load versus drift.

3.2 Joint panel shear behaviour

Linear potentiometers located on the joint panel are employed to calculate joint shear strain (as in [17], [22], [23]), according to Eq. (1):

$$\gamma_{joint,i} = \frac{\varepsilon_\theta - \varepsilon_x \cos^2\theta - \varepsilon_y \sin^2\theta}{\sin\theta\cos\theta} \quad (1)$$

where $\gamma_{joint,i}$ is the joint shear strain calculated by means of a certain set *i* of strain measures, ε_x and ε_z are strains in the horizontal and vertical directions, respectively, and ε_θ is the strain in the diagonal direction (with an angle of θ measured from the horizontal axis). Four estimates of the joint shear strain were obtained by four triangles of LPs located in the joint panel (see Figure 2). Joint shear strain was finally calculated as the mean of these four estimates. On the other hand, joint shear stress (τ_j) is calculated on the basis of equilibrium equations. In particular, joint shear demand V_{jh} is obtained depending on the beam load V_b, according to Eq. (2):

$$V_{jh} = \frac{V_b \cdot (L_b - h_c / 2)}{d^*} - \frac{V_b \cdot L_b}{2L_c} \quad (2)$$

where L_b is the beam shear length (up to the centerline of the columns), $(L_b-h_c/2)$ is the clear length of the beam, $2L_c$ represents the total length of bottom and top columns, d^* the internal lever arm of the beam section (evaluated herein as 0.9 times the effective depth, d, similarly to other literature studies, such as [12], [18], [20]). Joint shear stress can be finally calculated as the ratio between joint shear (V_{jh}) and joint horizontal area (A_{jh}).

In Figure 4, experimental responses in terms of $\tau_j/\sqrt{f_c}$ versus γ_{joint} are reported for all the tests. Data are represented until LPs measures are considered reliable (i.e. until cracks significantly involved the support points of LPs), namely until the end of the third sub-cycle at 3.00% drift for Test #1bP and Test #2bP, and until the end of the third sub-cycle at 2.00% drift for Test #1cP and Test #2cP.

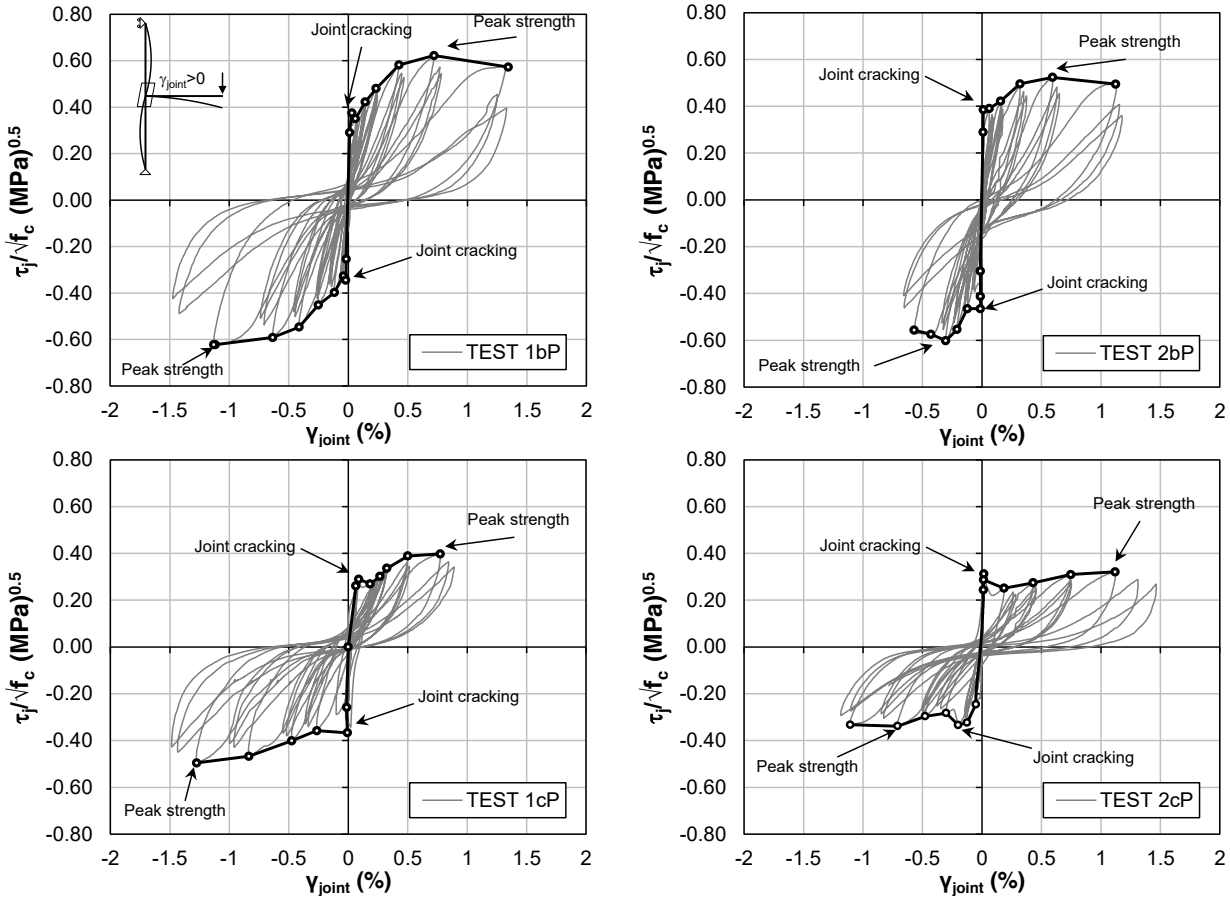

Figure 4: Joint panel response in terms of shear stress $\tau_j/\sqrt{f_c}$ – shear strain γ_j relationship.

3.3 Deformability contributions

The contributions due to joint, beam and columns to the overall deformability of each sub-assemblage are analyzed in this Section. First, the relationships between the imposed drift level and joint shear strain (γ_{joint}), rotation at beam/joint interface ($\theta_{s,b}$) and rotation at column/joint interface ($\theta_{s,c}$) - calculated at the end of the first sub-cycle for each imposed drift level - are evaluated. In particular, in Figure 5, joint shear strains are calculated and reported until significant cracks involved LPs supports, as explained in Section 4.1. Figure 5 also shows the rotation at beam (column)/joint interface (θ_s) – assumed as positive if clockwise –

as a function of the imposed drift for all the tests, evaluated for beam, top column and bottom column. Such rotations – and, thereby, their contribution to the overall deformability – are estimated through LPs located along the longitudinal bars of the columns at the interface with joint panel, and LVDTs located at beam-joint interface (see Figure 2). Starting from each pair of LPs or LVDTs (providing displacement lectures d_1 and d_2) located at a distance l, the rotation θ_s is calculated according to Eq. (3):

$$\theta_s = \frac{d_2 - d_1}{l} \tag{3}$$

Note that θ_s does not correspond exactly to the well-known "fixed-end rotation" since LPs provide the measure of the whole crack width at the interface, including the slippage of longitudinal bars both from the panel zone and from the element. Also in this case, the experimental data are plotted until the support points of the corresponding LPs and LVDTs were affected by significant cracks.

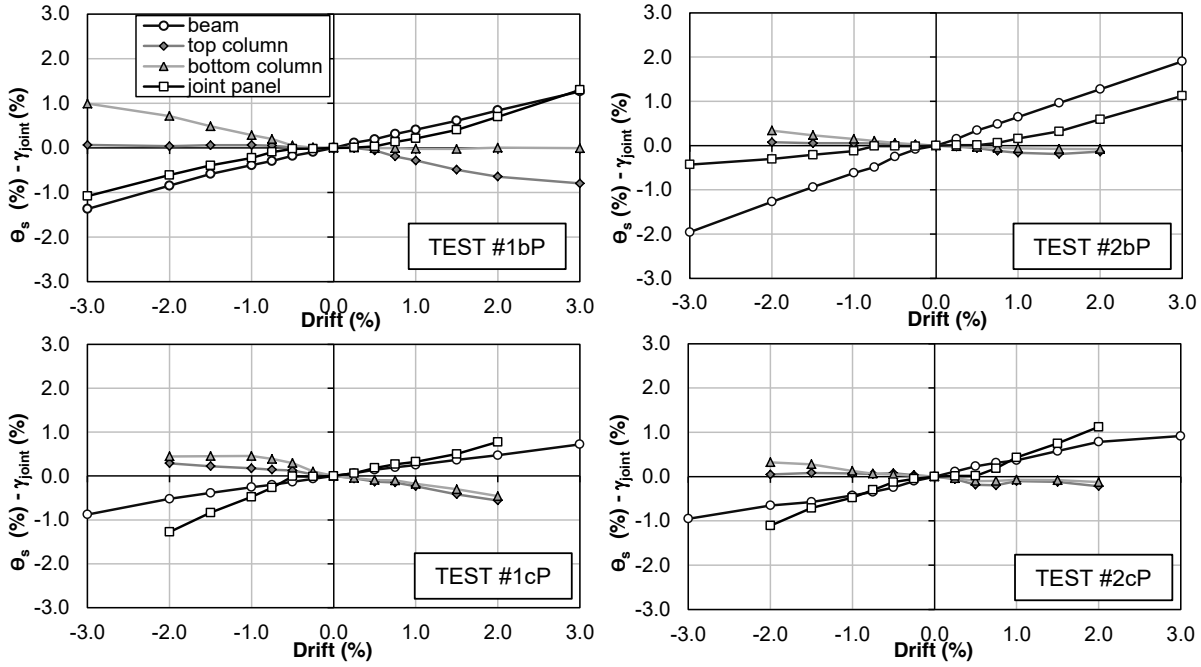

Figure 5: γ_{joint}, $\theta_{s,b}$ and $\theta_{s,c}$ versus global imposed drift.

4 NONLINEAR MODELLING

Experimental tests presented above have been numerically reproduced by means of OpenSees software [25]. In particular, starting from the adoption of the experimental shear stress-strain response for the joint panel, the contribution due to the slippage of longitudinal bars anchored into the joint core has been evaluated according to a bond model proposed in literature specifically for plain longitudinal bars.

Flexural response of beam and columns is modeled in a distributed plasticity approach. Concrete and steel properties were obtained from the test program reported in Section 2; Mander et al.'s model [26] was adopted for concrete and an elastic-plastic-hardening stress-strain relationship (Giuffre-Menegotto-Pinto steel material) was adopted for steel (*Concrete04* and *Steel02* uniaxial materials in OpenSees software, respectively). Shear response of the beam-column joint is modeled through the adoption of two rotational springs (see Figure 6): the first one is located in the centerline of the joint panel and it represents its shear behaviour;

the other ones are located at the interfaces between the joint and the adjacent beam/columns and represent the bond-slip contribution.

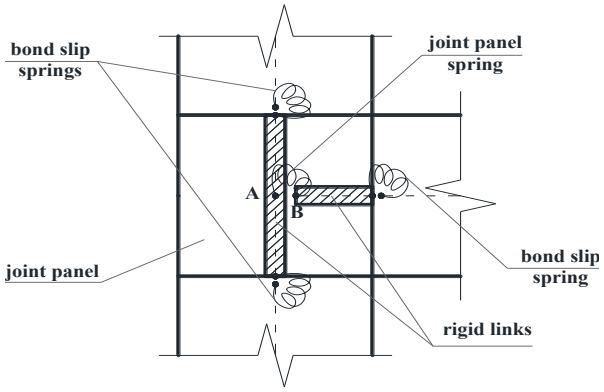

Figure 6: Numerical model for beam-column joint panel and bond slip.

4.1 Joint shear hysteretic behaviour

More in details, the joint panel zone model is a scissors model [27], implemented by defining duplicate nodes (A and B) with the same coordinates at the center of the joint panel and with rigid links spreading within the joint area. Node A is connected to the column rigid links and node B is connected to the beam rigid link. A zero-length rotational spring connects the two nodes and allows only relative rotation between them through a constitutive model which describes the shear deformation of the joint panel zone. Such a rotational spring is defined as a quadri-linear moment (M_j) – rotation (γ_j) spring characterized by four points, namely: cracking, pre-peak, peak and residual points. Therefore, the joint panel spring is implemented with a zero-length element defined by a four-point backbone moment-rotation relationship by the adoption of the *Pinching4* uniaxial material in OpenSees platform. M_j-γ_j relationship for joint panel is obtained herein by the experimental response in terms of joint shear stress-strain. Such experimental joint responses were first made symmetric (since specimens were all symmetrically reinforced) by averaging experimental shear stress and strain values between positive and negative loading directions at each drift level (see Figure7a). Then, these responses were quadri-linearized, clearly identifying the four required characteristic points introduced before (see Figure7b and Table 1).

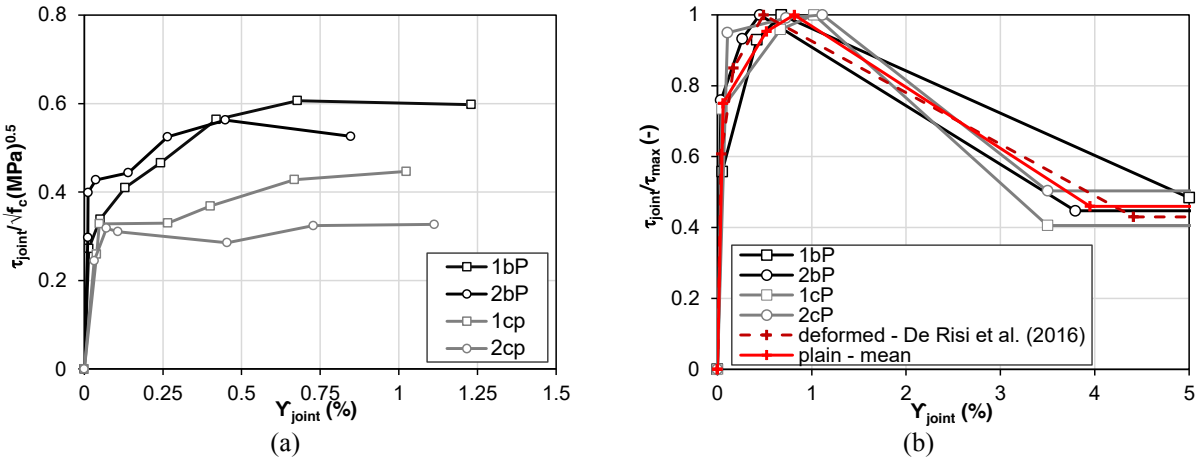

Figure 7: Averaged joint shear experimental response (a); quadri-linearized and normalized joint shear stresses for each test and comparison between mean joint shear responses of specimens with plain and deformed (from [28]) bars (b).

	$\tau_j/\tau_{j,max}$	γ_j (%)
Cracking	0.75	0.06
Pre-peak	0.95	0.52
Peak	1.00	0.82
Residual	0.46	4.20

Table 1: Quadri-linearized and normalized average joint shear stress-strain relationship.

For each test, the softening branch goes on up to the joint shear value corresponding to the beam load at the last imposed drift level. Note that, when experimental response of the joint panel was considered reliable only until the peak load is reached, joint shear strain corresponding to the end of the softening branch is properly calibrated to reproduce the experimentally observed softening stiffness on the global response (shown in Section 4.3).

The same tests adopted for the calibration of the backbone described above are used to calibrate the cyclic behaviour of the joint shear stress-strain response. The calibration is performed in OpenSees software on the basis of the hysteresis rules characterizing the *Pinching4* uniaxial material. As explained above, *Pinching4* is a uniaxial material belonging to the library of OpenSees. In particular, it allows modelling the cyclic degradation of unloading and reloading stiffness (through the parameters g_k and g_D, respectively), degradation in strength (through the parameters g_F) and pinching effects (through the parameters *rDisp*, *rForce* and *uForce*).

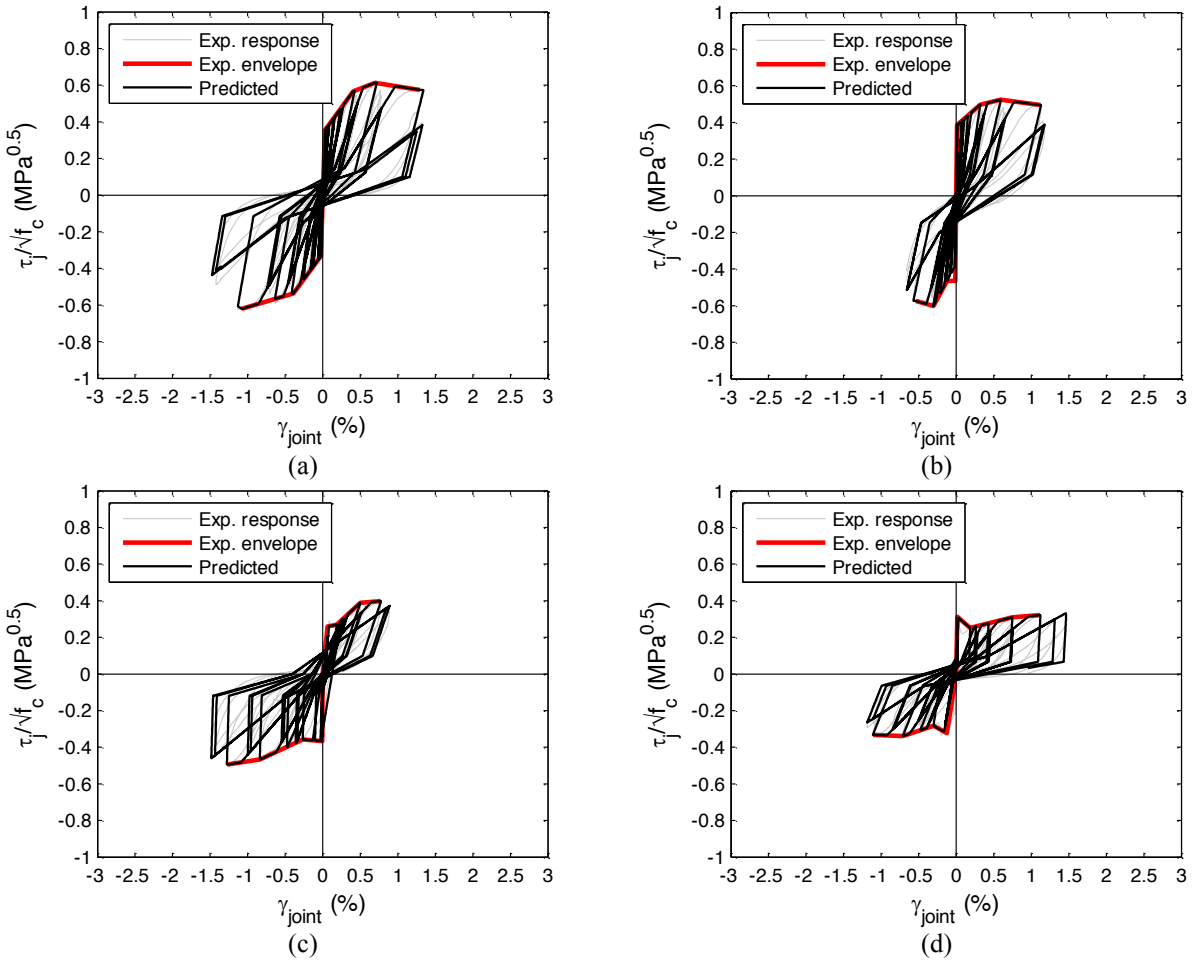

Figure 8: Joint panel: results of the calibration of the *Pinching4* hysteretic parameters for Tests #1bP (a), #2bP (b), #1cP (c), #2cP (d).

The calibration-phase of these key parameters was performed starting from the experimental shear stress-strain backbones and minimizing the error in terms of dissipated energy between the numerical and the experimental responses. No degradation in strength was introduced (namely all g_F parameters were set equal to zero) since it is already included in the backbone of the joint response obtained from experimental data. Figure 8 shows the comparison between numerical and experimental cyclic responses in terms of joint shear stress-strain. Finally, Table 2 reports the mean values of the calibrated parameters - later employed for the numerical simulations - adopted to fit the experimental response of the analyzed non-ductile exterior beam-column joints.

Joint shear panel					
Test #	**1pP**	**2bP**	**1cP**	**2cP**	**mean**
rDispP	0.30	0.30	-0.30	0.30	**0.23**
rDispN	0.30	0.30	0.30	0.30	
rForceP	0.25	0.25	0.05	0.30	**0.23**
rForceN	0.25	0.25	0.25	0.20	
uForceP	-0.20	-0.20	-0.30	-0.20	**-0.21**
uForceN	-0.20	-0.20	-0.20	-0.20	
gK_1	0.85	0.85	0.70	0.60	**0.75**
gK_{lim}	0.96	0.96	0.96	0.96	**0.96**
gD_1	0.50	0.50	0.30	0.30	**0.40**
gD_3	0.50	0.50	0	0	**0.25**
gD_{lim}	0.70	0.70	0.70	0.70	**0.70**
gF_i (i=1,..4)	0	0	0	0	**0**
gE	100	100	100	100	**100**

$gK_1=gK_2=gK_3=gK_4=0$; $gD_2=gD_4=0$

Table 2: Results of the calibration of joint panel hysteretic behaviour through Pinching4 material.

4.2 Fixed-end-rotation hysteretic behaviour

Deformability contribution due to the slippage of beam/columns longitudinal bars anchored into the joint core is reproduced through another zero-length element introduced at beam/columns-joint interface. The related M-θ_s relationship is calculated using an analytical bond-slip model from literature. A very limited number of studies are available in the literature on bond–slip mechanisms in structural elements with plain bars (e.g. [29]-[33]) with respect to deformed bars. Certainly, very low values for the maximum bond strength (τ_{max}) are proposed both in literature and codes due to the bad quality of the concrete-steel interaction (e.g. τ_{max} equal to $0.15\cdot\sqrt{f_c}$ or $0.30\cdot\sqrt{f_c}$ are suggested by CEB-Fib [34] in "poor" and "good" bond conditions, respectively).

In this Section, the attention is focused on the fixed-end-rotation at beam-joint interface (see Figure 9), since this deformability contribution is always preeminent with respect to that due to the columns. In order to calculate the M-θ_s relationship, the cyclic moment-curvature relationship (M-ϕ) is calculated first, under a given imposed cyclic path of curvatures. Then, for each value of ϕ, the slip (s) at the loaded end of the anchored bars is evaluated at top and bottom layers as a function of the corresponding strain (ε) in the reinforcement. To this end, the finite difference method is applied, discretizing the straight portion (l_d) of the anchored bar in a number of sub-portions of equal length; then, the problem is solved using equilibrium and

compatibility equations at each section of the discretized bar, employing the stress-strain constitutive relationship of the reinforcement steel and the bond strength-slip cyclic relationship proposed by Verderame et al. [31]. The hook deformability contribution is taken into account by means of the $\sigma_{s,h}$-s_h relationship by Fabbrocino et al. [29], with hysteresis rules assumed according to [34]. Then, the rotation θ_s corresponding to the calculated slip in top and bottom reinforcement layers is evaluated as the difference between the two slip values (s_{in}-s_{out}) divided by the distance between the reinforcement layers. According to this procedure, the M-θ_s responses (grey lines in Figure 10) are calculated for each test.

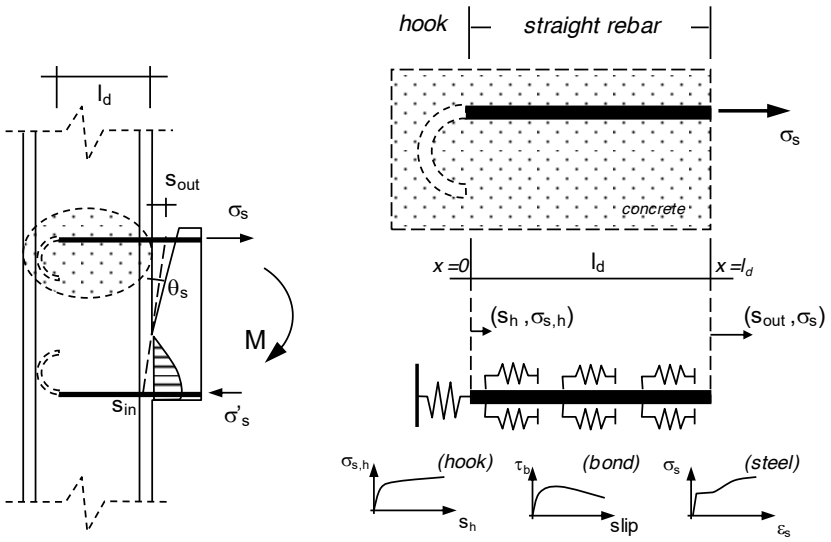

Figure 9: Evaluation of the fixed-end-rotation contribution (adapted from [35])

Fixed-end-rotation					
Test #	**1pP**	**2bP**	**1cP**	**2cP**	**mean**
rDispP	0.70	0.78	0.75	0.80	**0.76**
rDispN	0.70	0.78	0.75	0.80	
rForceP	0.70	0.78	0.75	0.80	**0.76**
rForceN	0.70	0.78	0.75	0.80	
gK_1	0.82	0.89	0.85	0.91	**0.87**
gK_{lim}	0.99	0.99	0.99	0.99	**0.99**
gD_{lim}	0.99	0.99	0.99	0.99	**0.99**
gF_i (i=1,..4)	0	0	0	0	**0**
gE	100	100	100	100	**100**

gK_1=gK_2=gK_3=gK_4=0; gD_1=gD_2=gD_3=gD_4=0; uForceP=uForceN=0

Table 3: Results of the calibration of fixed-end-rotation hysteretic behaviour through *Pinching4* material.

Then, the calibration-phase of the key parameters of Pinching4 material for fixed-end-rotation springs is performed starting from such relationships used as a reference, and minimizing the error in terms of dissipated energy between the numerical and the experimental responses, as explained in Section 4.1 for joint shear behaviour. Figure 10 shows the comparison between numerical responses obtained by using the *Pinching4* uniaxial material in OpenSees (black dotted line) and numerical cyclic responses in terms of M-θ_s obtained by the adoption of the bond cyclic model proposed by Verderame et al. [31] (grey solid line) and

used as a reference. Finally, Table 3 reports the mean values of the calibrated parameters - later employed for the numerical simulations.

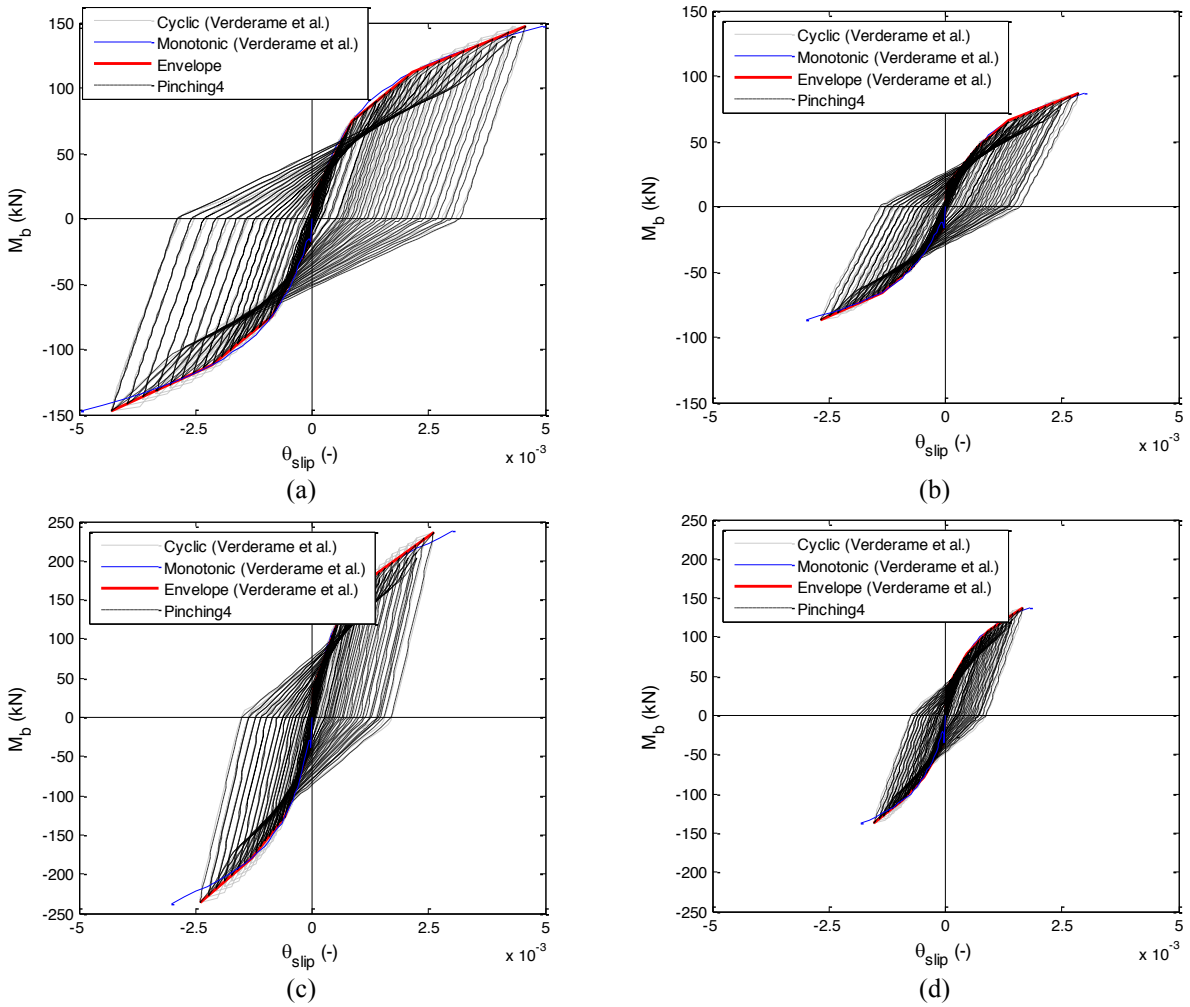

Figure 10: Fixed-end-rotation: results of the calibration of the *Pinching4* parameters for Tests #1bP (a), #2bP (b), #1cP (c), #2cP (d).

4.3 Numerical-versus-experimental comparisons

The comparisons between experimental responses and numerical simulations based on the assumptions explained in Section 4.1 and 4.2 are finally shown in Figure 11. From these comparisons, it can be observed that:

- elastic stiffness is well reproduced, even if this stiffness does not depend on the slip deformability contribution, since such a contribution becomes relevant only after beam cracking (namely, only after a first reduction in the slope of the global response);
- global deformability is slightly underestimated at peak load;
- nevertheless, bond stress-slip model by Verderame et al. [31], in conjunction with the model by Fabbrocino et al. [29] for the hook, results a good model to reproduce the contribution of bond slip to the global response;
- the numerical responses well reproduce also softening stiffness and residual strength, thanks to the calibration of such parameters (graphically reported in Figure 7b).

- numerical hysteretic responses well predict unloading and reloading stiffness degradation and pinching effect for all the investigated tests.

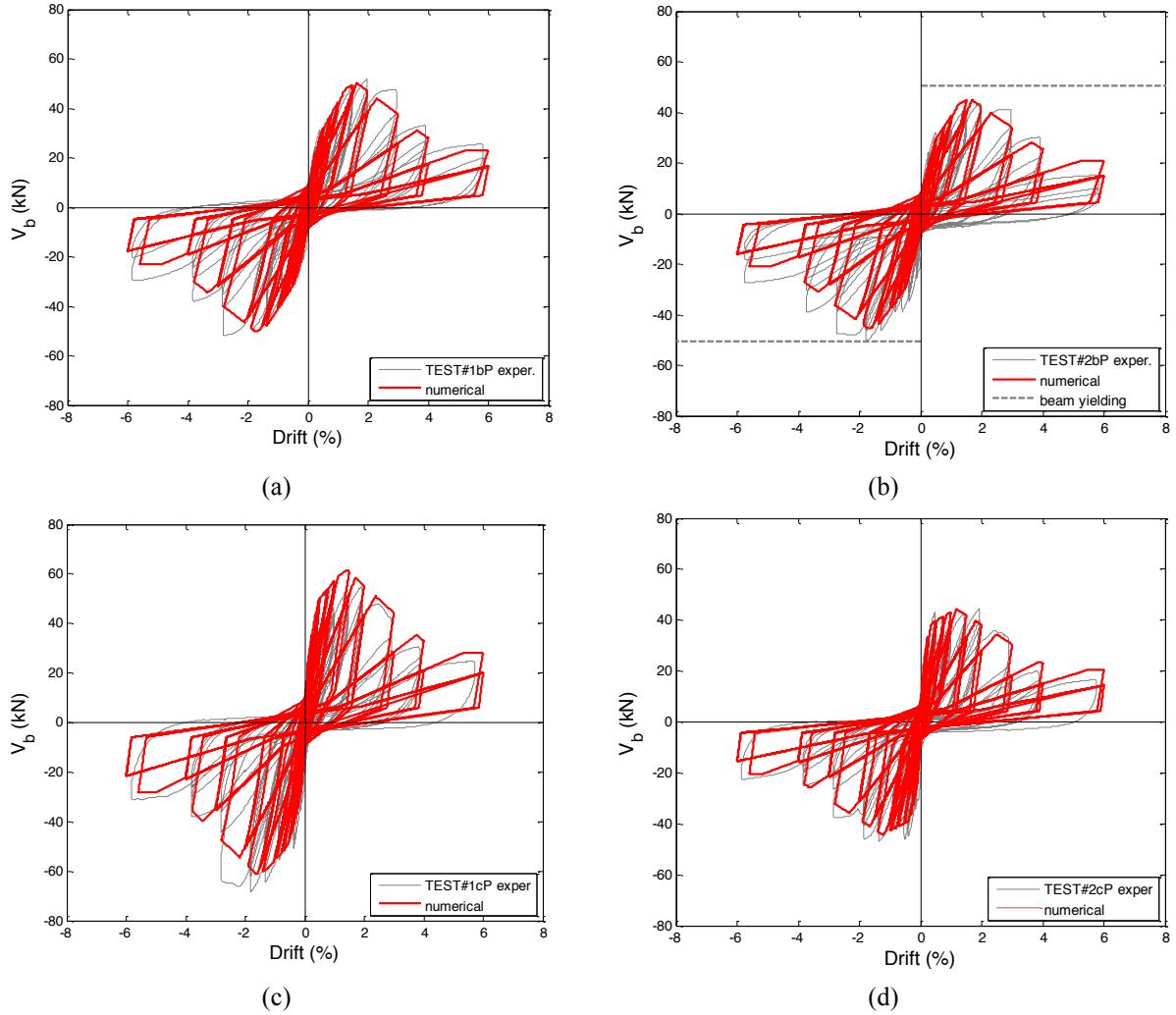

Figure 11: Experimental versus numerical comparisons

5 CONCLUSIONS

In the present work, experimental results related to four tests on unreinforced exterior RC beam-column joints with hook-ended longitudinal plain bars were shown and analyzed. The specimens differ for joint aspect ratio and beam longitudinal reinforcement amount, since one of the main aims of the work was to observe and analyze the effect of such parameters on joint shear strength and deformability for this joint typology.

About experimental joint shear strength, it was observed that: being equal aspect ratio, the higher the beam longitudinal reinforcement amount the higher joint shear strength; whereas, being equal beam longitudinal reinforcement amount, the higher the joint aspect ratio the lower joint shear strength.

The analysis of local responses highlighted that, being equal joint aspect ratio, the lower the beam longitudinal reinforcement ratio, the higher the deformability contribution due to rotation at beam/joint interface. Furthermore, being equal beam longitudinal amount, the contribution due to rotation at beam/joint interface to the overall deformability increases if the joint aspect ratio (in particular, beam high) decreases.

Finally, the modelling approach adopted to reproduce experimental envelopes resulted in a quite good accordance with experimental results. Numerical hysteretic responses well predicted unloading and reloading stiffness degradation and pinching effect for all the investigated tests. Nevertheless, further efforts in future works should be performed to:

- validate the numerical modelling approach presented herein through simulations of a higher number of similar specimens, experimentally tested and presented in literature;
- reproduce the cyclic behaviour of the specimens by calibrating a constant value of bond strength (similarly to that proposed by Sezen and Setzler [36] for deformed bars), which is properly calibrated for plain bars and can be applied easier in numerical modelling.

Acknowledgements

This work was developed under the financial support of METROPOLIS ("Metodologie e tecnologie integrate e sostenibili per l'adattamento e la sicurezza di sistemi urbani" - PON 'Ricerca e Competitività 2007 – 2013) and "ReLUIS-DPC 2014-2018 PR 2- Linea Strutture in cemento armato", funded by the Italian Department of Civil Protection (DPC). These supports are gratefully acknowledged.

REFERENCES

[1] S. Park and K.M. Mosalam, Simulation of Reinforced Concrete Frames with Nonductile Beam-Column Joints, *Earthquake Spectra*, **29**(1), 233-257, 2013

[2] O.C. Celik and B.R. Ellingwood, Modeling Beam-Column Joints in Fragility Assessment of Gravity Load Designed Reinforced Concrete Frames, *Journal of Earthquake Engineering*, **12**, 357-381, 2008.

[3] C. Menna, R. Frascadore, C. Moroni, G.P. Lignola, G. De Martino, A. Salzano, M. Di Ludovico, A. Prota, G. Manfredi, E. Cosenza, Rapporto fotografico relativo ai danni subiti da alcuni edifici a seguito del sisma del centro Italia del 2016, in Italian.

[4] J.P. Moehle and S.A. Mahin, Observations on the behavior of reinforced concrete buildings during earthquakes, Earthquake-Resistant Concrete Structures Inelastic Response and Design SP-127, American Concrete Institute, ed. S.K. Ghosh, Detroit, 1991.

[5] P. Ricci, F. De Luca, G.M. Verderame, 6th April 2009 L'Aquila earthquake, Italy: reinforced concrete building performance, *Bulletin of Earthquake Engineering*, **9**(1), 285-305, 2011.

[6] C. Clyde, C.P. Pantelides, L.D. Reaveley, Performance-Based Evaluation of Exterior Reinforced Concrete Buildings Joints for Seismic Excitation, PEER Report, No. 2000/05, Pacific Earthquake Engineering Research Center, University of California, Berkeley, USA, 2000.

[7] C.P. Pantelides, J. Hansen, J. Nadauld, L.D. Reaveley, Assessment of Reinforced Concrete Building Exterior Joints with Substandard Details, PEER Report, No. 2002/18, Pacific Earthquake Engineering Research Center, University of California, Berkeley, USA, 2002.

[8] A.G. Tsonos and K.V. Papanikolaou, Post-Earthquake Repair and Strengthening of Reinforced Concrete Beam-Column Connections (Theoretical & Experimental Investigation), *Bulletin-New Zealand society for earthquake engineering*, **36**(2), 73-93, 2003

[9] H. F. Wong, Shear strength and seismic performance of non-seismically designed RC beam–column joints, Ph.D. thesis. Hong Kong University of Science and Technology, 2005.

[10] A. Masi, G. Santarsiero, and D. Nigro, Cyclic tests on external RC beam-column joints: role of seismic design level and axial load value on the ultimate capacity, *Journal of Earthquake Engineering*, **17**(1), 110-136, 2013.

[11] A. Liu, Seismic assessment and retrofit of pre-1970s reinforced concrete frame structures, 2001.

[12] P. Ricci, M.T. De Risi, G.M. Verderame, G. Manfredi, Experimental tests of unreinforced exterior beam-column joints with plain bars, *Engineering Structures*, **118**, 178-194, 2016.

[13] J.S. Jeon, A. Shafieezadeh, R. DesRoches, Statistical models for shear strength of RC beam-column joints using machine-learning techniques, *Earthquake Engineering and Structural Dynamics*, **43**(14), 2075-2095, 2014.

[14] S. Pampanin, G.M. Calvi, and M. Moratti, Seismic behavior of RC beam-column joints designed for gravity only. 12th European Conference on Earthquake Engineering, paper n.726, London 2002, 2002.

[15] G. Metelli, F. Messali, C. Beschi, and P. Riva, A model for beam–column corner joints of existing RC frame subjected to cyclic loading, *Engineering Structures*, **89**, 79-92, 2015.

[16] Circolare LL.PP. 617/2009, 2 febbraio 2009, n. 617 Istruzioni per l'applicazione delle «Nuove norme tecniche per le costruzioni» di cui al decreto ministeriale 14 gennaio 2008, in Italian.

[17] M. T. De Risi, P. Ricci, G.M. Verderame and G. Manfredi, Experimental assessment of unreinforced exterior beam–column joints with deformed bars. *Engineering Structures*, **112**, 215-232, 2016.

[18] G.M. Verderame, M.T. De Risi, P. Ricci, Experimental investigation of unreinforced exterior beam-column joints with plain and deformed bars. *Journal of Earthquake Engineering*, published online on 29/09/2016.

[19] M.J.N. Priestley, Myths and fallacies in earthquake engineering, revisited. The Mallet Milne Lecture. IUSS Press: Pavia, Italy, 2003.

[20] S. Park and K.M. Mosalam, Analytical model for predicting the shear strength of unreinforced exterior beam-column joints, *ACI Structural Journal* **109**, 149–159, 2012.

[21] CEN, 1998-1, Eurocode 8, Design of structures for earthquake resistance – Part 1: General rules, seismic actions and rules for buildings. European Committee for Standardization, Brussels, Belgium, 2010.

[22] M. Engindeniz, Repair and Strengthening of Pre-1970 Reinforced Concrete Corner Beam-Column Joints Using CFRP Composites, PhD Thesis, Civil and Environmental Engineering Department, Georgia Institute of Technology, August 2008.

[23] W.M. Hassan, Analytical and Experimental Assessment of Seismic Vulnerability of Beam-Column Joints without Transverse Reinforcement in Concrete Buildings, PhD Dissertation, University of California, Berkeley, California, USA, 2011.

[24] ASCE/SEI 41, Seismic rehabilitation of existing buildings. American Society of Civil Engineers, Reston, VA, USA, 2007.

[25] F. McKenna, G.L. Fenves, M.H. Scott, OpenSees: Open System for Earthquake Engineering Simulation. Pacific Earthquake Engineering Research Center. University of California, Berkeley, CA, USA, 2010, available at http://opensees.berkeley.edu.

[26] J.B. Mander, M.J.N. Priestley and R. Park, Theoretical stress-strain model for confined concrete. *ASCE, Structural Engineering*, **114**(8), 1804-1826, 1988.

[27] S. Alath, S.K. Kunnath, Modelling inelastic shear deformations in RC beam–column joints. Engineering mechanics proceedings of 10th conference, May 21–24, University of Colorado at Boulder, Boulder, Colorado, vol. 2. New York: ASCE: p. 822–5, 1995.

[28] M.T. De Risi, P. Ricci, G.M. Verderame, Modelling exterior unreinforced beam-column joints in seismic analysis of non-ductile RC frames, *Earthquake Engineering and Structural Dynamics*, published online on 08/11/2016 (doi: 10.1002/eqe.2835);

[29] G. Fabbrocino, G.M. Verderame, G. Manfredi, E. Cosenza, Structural models of critical regions in old-type RC frames with smooth rebars, *Engineering Structures* **26**(14), 2137-2148, 2004.

[30] G.M. Verderame, P. Ricci, G. De Carlo, and G. Manfredi G., Cyclic bond behaviour of plain bars. Part I: Experimental investigation, *Construction and Building Materials*, **23**(12), 3499-3511, 2009.

[31] G.M. Verderame, De Carlo G, Ricci P and Fabbrocino G., Cyclic bond behaviour of plain bars. Part II: Analytical investigation, *Construction and Building Materials*, **23** (2009), pp. 3512-3522, 2009.

[32] J. Melo, T. Rossetto, and H. Varum, Experimental study of bond–slip in RC structural elements with plain bars, *Materials and Structures*, **48**(8): 2367-2381, 2014.

[33] C. Fernandes, J. Melo, H. Varum, and A. Costa, Cyclic behavior of substandard reinforced concrete beam-column joints with plain bars, *ACI Structural Journal*, **110**, 1,137, 2013.

[34] CEB Fib - Model Code 2010 - first complete draft. Fédération Internationale du Béton fib/International Federation for Structural Concrete.

[35] G. Fabbrocino, G.M. Verderame, G. Manfredi, Experimental behaviour of straight and hooked smooth bars in existing RC. buildings. 12th European Conference on Earthquake Engineering, Paper n. 393, London (UK), 2003.

[36] H. Sezen and E.J. Setzler, Reinforcement slip in reinforced concrete columns. *ACI Structural Journal*, **105**(3), 2008.